The matching pursuit approach based on the modulated Gaussian pulse for efficient guided wave damage detection

Article *in* Smart Materials and Structures · May 2005

DOI: 10.1088/0964-1726/14/4/013

3 authors, including:

Kyung ho Sun
Korea Institute of Machinery and Materials
17 PUBLICATIONS **197** CITATIONS
SEE PROFILE

Yoon Young Kim
Seoul National University
310 PUBLICATIONS **2,900** CITATIONS
SEE PROFILE

The matching pursuit approach based on the modulated Gaussian pulse for efficient guided-wave damage inspection

2005 Smart Mater. Struct. 14 548

(http://iopscience.iop.org/0964-1726/14/4/013)

INSTITUTE OF PHYSICS PUBLISHING SMART MATERIALS AND STRUCTURES
Smart Mater. Struct. **14** (2005) 548–560 doi:10.1088/0964-1726/14/4/013

The matching pursuit approach based on the modulated Gaussian pulse for efficient guided-wave damage inspection

Jin-Chul Hong, Kyung Ho Sun and Yoon Young Kim[1]

School of Mechanical and Aerospace Engineering and National Creative Research Initiatives Center for Multiscale Design, Seoul National University, Shinlim-Dong, San 56-1, Kwanak-Gu, Seoul 151-742, Korea

E-mail: jchong@idealab.snu.ac.kr, suniekh@idealab.snu.ac.kr and yykim@snu.ac.kr

Received 18 May 2004, in final form 7 October 2004
Published 4 May 2005
Online at stacks.iop.org/SMS/14/548

Abstract
The success of the guided-wave damage inspection technology depends not only on the generation and measurement of desired waveforms but also on the signal processing of the measured waves, but less attention has been paid to the latter. This research aims to develop an efficient signal processing technique especially suitable for the current guided-wave technology. To achieve this objective, the use of a two-stage matching pursuit approach based on the Gabor dictionary is proposed. Instead of truncated sine pulses commonly used in waveguide inspection, Gabor pulses, the modulated Gaussian pulses, are chosen as the elastic energy carrier to facilitate the matching pursuit algorithm. To extract meaningful waves out of noisy signals, a two-stage matching pursuit strategy is developed, which consists of the following: rough approximations with a set of predetermined parameters characterizing the Gabor pulse, and fine adjustments of the parameters by optimization. The parameters estimated from measured longitudinal elastic waves can be then directly used to assess not only the location but also the size of a crack in a rod. For the estimation of the crack size, in particular, Love's theory is incorporated in the matching pursuit analysis. Several experiments were conducted to verify the validity of the proposed approach in damage assessment.

(Some figures in this article are in colour only in the electronic version)

1. Introduction

The guided-wave inspection technology has been widely used for long-range damage detection [1–5]. Compared to standard ultrasonic technology, it can cover a wider range by propagating elastic pulses along waveguides and capturing the reflected pulses from the damage in waveguides. Therefore, the technology requires efficient methods to generate and receive elastic pulses in waveguides. It also requires the appropriate signal processing of measured signals for the estimation of damage location and size. In order to detect small cracks, one needs a sophisticated signal processing technique, which is the subject of this investigation.

When a crack existing in a waveguide is small, it is difficult to extract damage information directly from the measured signals. In this situation, one may use the time domain approaches [6, 7] based on cross-correlations and the Hilbert transform, or the frequency domain approaches [8] based on spectral analysis. Although both approaches are sensitive to the noise effect and the dispersion phenomenon, they have been partly successful in identifying cracks and estimating their locations, but not so successful in estimating crack size. For the size estimation, more information should be extracted from measured signals than that needed for the location estimation.

[1] Author to whom any correspondence should be addressed.

In addition, some efficient theoretical model for wave reflection is also needed for the size estimation. Consequently, a more advanced signal processing technique is required for effective damage inspection.

The objective of this investigation is to develop an efficient signal processing technique especially effective for wave signals measured by the guided-wave technology. The key concept of the proposed signal processing technique is to develop a two-stage matching pursuit algorithm to accurately extract meaningful pulses out of noisy signals. Furthermore, the pulse generated by the wave transmitter is so designed to minimize the distortion by dispersion and to adaptively facilitate the matching pursuit algorithm. The selected pulse is a Gabor function, i.e., a modulated Gaussian function having a prescribed center frequency and time spread property. This function has an excellent energy concentration property both in time and frequency.

The Gabor function is expressed as

$$f(t) = Ag\left(\frac{t-u}{\sigma}\right)\cos[2\pi\xi(t-u)+\phi],$$
$$g(t) = \pi^{-1/4}\mathrm{e}^{-t^2/2}.$$

This function is characterized by a set γ of five parameters (A: amplitude, σ: spread in the time axis, ξ: center frequency, u: time delay, ϕ: phase shift). If the incident pulse into a waveguide is a Gabor function, the signal measured by the receiver can also be represented by one or some Gabor functions. The measured signals are usually noisy and somewhat distorted by dispersion, so a matching pursuit algorithm based on the Gabor dictionary was used to accurately estimate the sets γs consisting of the parameters A, u, σ, ξ, and ϕ.

The existing matching pursuit approach [9–11] has been mainly developed for signal compression and approximation. In this investigation, a two-stage matching pursuit algorithm is developed to accurately estimate parameters characterizing pulses which are then used for the estimation of damage location and size. In the first stage, γ is estimated from a finite space of a pre-selected uniformly distributed parameter set. In the second stage, an optimization method is used to update the parameter set where the set determined in the first stage is used as an initial guess. This two-stage procedure is repeated through all iterations.

In the present investigation, longitudinal waves in a rod are mainly used for all experiments. Since the longitudinal wave is dispersive, the shapes of the measured echoes are somewhat different from that of the Gabor pulse generated by the transducer. However, the present Gabor function-based matching pursuit algorithm is not affected by such dispersion unless the echo is overly distorted. Once the parameter sets are determined by the matching pursuit algorithm, the estimation of the crack in a waveguide is rather straightforward.

To assess the crack size from the measured signals, wave mechanics such as reflection as well as the dispersion characteristics must be known. Though the exact Pochhammer–Chree dispersion equation is available, a simplified theory given by Love for longitudinal wave propagation will be employed to efficiently assess the crack size.

The effectiveness of the proposed method is checked both by numerical simulations and by experimental results. For experimental work, rods with small partial cracks of different size are used. Among various transducers, the magnetostrictive transducers are employed for the present experiments.

2. Proposed guided-wave damage inspection method

2.1. The choice of initial pulse shape

For efficient damage inspection, it is important to use a wave pulse having good time and frequency localization. When the pulse is not localized in frequency, the pulse can be considerably dispersed unless non-dispersive wave modes are excited.

Consider the common pulse form used in many applications, which takes on truncated sines:

$$f_{\mathrm{sp}}(t) = \begin{cases} \sin(2\pi\xi t) & 0 \leqslant t \leqslant \frac{k}{\xi} \\ 0 & \text{otherwise.} \end{cases} \tag{1}$$

In equation (1), t is time and ξ is the center frequency. The time support of the pulse $f_{\mathrm{sp}}(t)$ is adjusted by k. Figure 1(a) shows $f_{\mathrm{sp}}(t)$ for $k = 3$ and $\xi = 100$ kHz, and figure 1(b), its Fourier transform. Though the pulse $f_{\mathrm{sp}}(t)$ has very simple form, it has undesirable properties. Since the waveform is uniformly distributed over a certain time support, its time localization is not so good. In addition, the energy of the pulse is not so concentrated on the center frequency as can be seen from figure 1(b). This is due to the abrupt rise and fall at the head and the tail of the pulse. Consequently, the pulse can become considerably dispersed as it propagates.

To overcome the bad time and frequency localization, we use a modulated Gaussian pulse (also known as the Gabor pulse) $f_{\mathrm{Gp}}(t)$:

$$f_{\mathrm{Gp}}(t) = \mathrm{e}^{-t^2/2\sigma^2}\cos(2\pi\xi t+\phi) \tag{2}$$

where σ controls the (effective) time width of the pulse. The main motivation of using $f_{\mathrm{Gp}}(t)$ is that the Gabor waveform has the best time–frequency resolution [12]. Figure 2 shows a typical Gabor waveform with $\sigma = 8\times10^{-6}$ s ($=40\Delta t$; Δt: sampling time), $\xi = 100$ kHz, and $\phi = 0$ rad. Although the time support ($\approx 6s\,\Delta t$) of the Gabor pulse is slightly longer than that of $f_{\mathrm{sp}}(t)$, the time localization of the Gabor pulse is better because the pulse energy is concentrated near the center. This good localization property is very useful in pinpointing the arrival time of the pulse. Furthermore, the effect of dispersion is not so severe with the Gabor pulse because its energy is concentrated at the center frequency: compare figures 1(b) and 2(b). By controlling the time width σ, one may find the best form of the Gabor pulse for given damage detection problems.

2.2. Proposed matching pursuit approach based on the Gabor dictionary

Before proposing a new approach for analyzing the reflected pulse for damage identification, the reason for using the Gabor pulse-based matching pursuit will be stated.

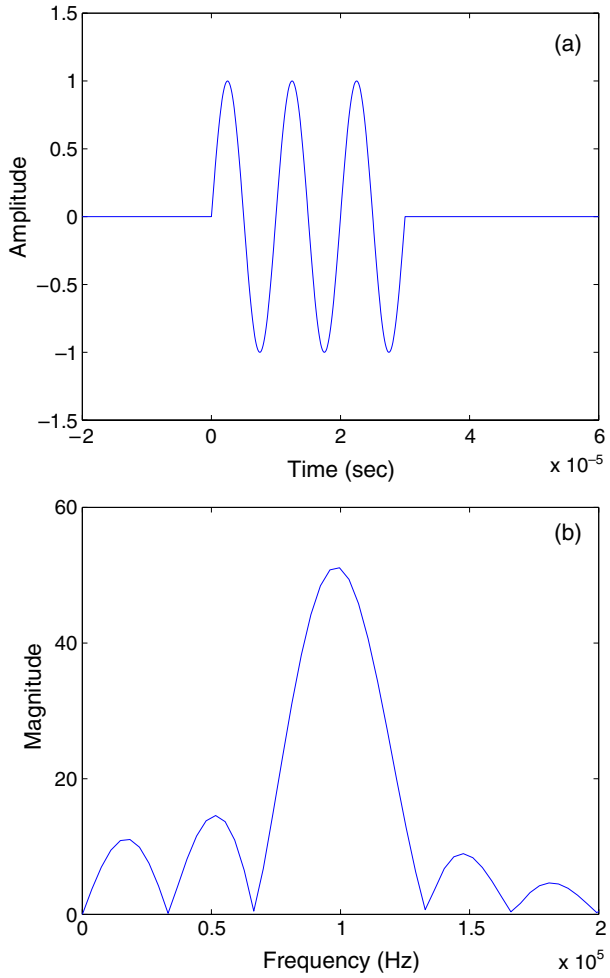

Figure 1. The pure sine pulse $f_{\mathrm{sp}}(t)$. (a) The shape of the sine pulse in the time domain and (b) the magnitude of its Fourier transform $F_{\mathrm{sp}}(\omega)$.

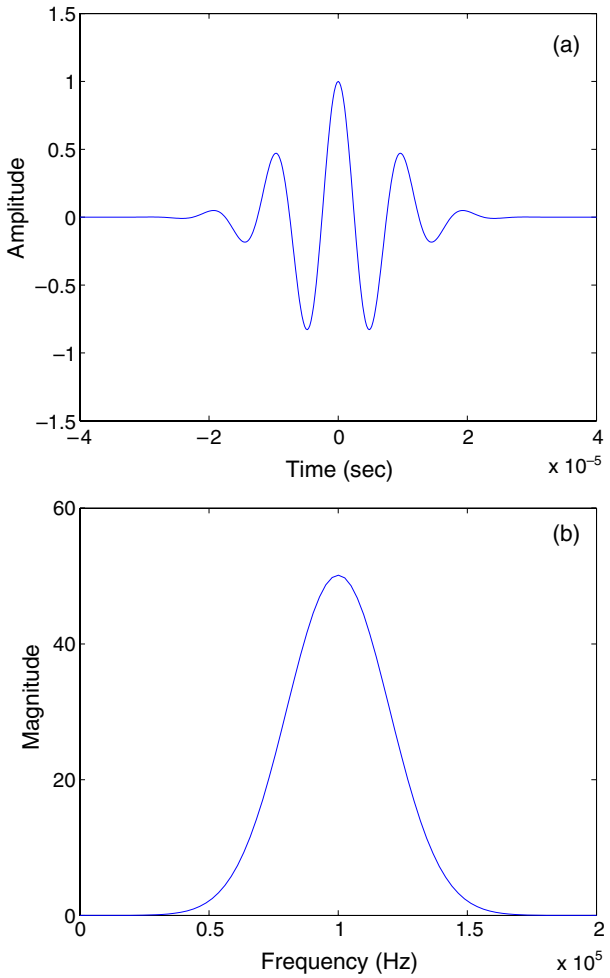

Figure 2. The modulated Gaussian pulse $f_{\mathrm{Gp}}(t)$. (a) The shape of the modulated Gaussian pulse in the time domain and (b) the magnitude of its Fourier transform $F_{\mathrm{Gp}}(\omega)$.

Assume that a pulse $s_{\mathrm{in}}(t)$ is a Gabor pulse generated by a transducer and propagates along a waveguide. If the pulse is reflected by a reflector such as a crack, the reflected pulse $s_{\mathrm{ref}}(t)$ can be written as

$$s_{\mathrm{ref}}(t) = \frac{1}{2\pi}\int_{-\infty}^{+\infty} R(\omega)\, S_{\mathrm{in}}(\omega) \mathrm{e}^{\mathrm{j}\omega t}\, \mathrm{d}\omega \tag{3}$$

where $S_{\mathrm{in}}(\omega)$ is the Fourier transform of $s_{\mathrm{in}}(t)$. The reflection coefficient $R(\omega)$ is frequency dependent, which can be expressed as

$$R(\omega) = |R(\omega)|\mathrm{e}^{\mathrm{j}\theta(\omega)} \tag{4}$$

where $\theta(\omega)$ denotes the phase shift. Equations (3) and (4) imply that $s_{\mathrm{ref}}(t)$ is an amplitude-attenuated and phase-shifted version of the input pulse. If the dispersion is not severe for the frequency range of interest, the reflection coefficient $R(\omega)$ is nearly independent of frequency. In this case, the reflected pulse $s_{\mathrm{ref}}(t)$ will not be much different from the input pulse (except in phase).

Consequently, the reflected pulse may be well approximated by some modifications of the input Gabor pulse. For instance, the adjustment of u, σ, and ϕ in $s_{\mathrm{in}}(t)$ will give a good approximation to $s_{\mathrm{ref}}(t)$. To carry out this approximation process efficiently and accurately, we propose to use the matching pursuit algorithm.

The matching pursuit algorithm [9] iteratively projects a signal onto a given dictionary and chooses the dictionary atom that best matches the signal at each iteration. If the dictionary is so selected to represent well the characteristics of a given signal, only a few atoms will be required for the signal representation.

Therefore, in this work, we will employ the Gabor dictionary: the Gabor dictionary $D = \{g_\gamma\}_{\gamma\in\Gamma}$ (Γ: a set of possible parameters which will be explained later) is defined in terms of the following real-valued Gabor functions:

$$g_\gamma(t) = w\left(\frac{t-u}{\sigma}\right)\cos(2\pi\xi(t-u)+\phi) \tag{5a}$$

$$= w\left(\frac{t-u}{s\,\Delta t}\right)\cos(2\pi\xi(t-u)+\phi) \tag{5b}$$

where $w(t) = \mathrm{e}^{-t^2/2}$ is the Gaussian window and the time width σ in equation (5*a*) is replaced by $s\,\Delta t$ in equation (5*b*). Note that the shape and the location in the time axis are completely characterized by the set $\gamma = (u, s, \xi, \phi)$.

The matching pursuit algorithm is an iterative greedy approach, which is explained below. Let $f(t)$ be the signal to be analyzed. Then $f(t)$ is decomposed into the following form after M iterations:

$$f = \sum_{i=1}^{M} A_i g_{\gamma_i} + R^{M+1} f = \sum_{i=1}^{M} \frac{\langle R^i f, g_{\gamma_i}\rangle}{\|g_{\gamma_i}\|^2} g_{\gamma_i} + R^{M+1} f \tag{6}$$

where the amplitude of the expansion is denoted by A_i and $R^{M+1} f$ is the residual after M iterations. The optimal form of the Gabor function $g_{\gamma_i}(t)$ at the ith iteration is determined as

$$g_{\gamma_i} = \arg\max_{g_{\gamma_i} \in D} \frac{|\langle R^i f, g_{\gamma_i}\rangle|}{\|g_{\gamma_i}\|^2}. \tag{7}$$

In theory, the parameter space of the Gabor functions is infinite and $R^{M+1} f$ approaches zero if M goes to infinity. Since excessively large M is impractical, finding a good estimate for g_{γ_i} may be important to expedite the iterative process. So, we have developed a two-phase search method described below.

Phase I. To efficiently evaluate the phase shift ϕ, the following complex-valued Gabor function $\tilde{g}_{(u,s,f)}$, not the real-valued Gabor function $g_{(u,s,f,\phi)}$, is used:

$$\tilde{g}_{(u,s,f)} = w\left(\frac{t-u}{s\Delta t}\right) \mathrm{e}^{\mathrm{i}2\pi\xi(t-u)}. \tag{8}$$

The sub-optimal parameter $\tilde{\gamma}_i = (u_i, s_i, \xi_i)$ is searched within a pre-selected subspace $\tilde{\Gamma}(u, s, \xi)$. The parameter u_i is selected among the sampled times and s_i among some uniformly distributed values which are determined with the consideration of the initially transmitted pulse width. The center frequency of the transmitted pulse is an excellent guess to ξ_i, so the procedure for finding ξ_i may be skipped. Then, the sub-optimal elementary Gabor function $\tilde{g}$ is determined from

$$\tilde{g}_{(u_i,s_i,\xi_i)} = \arg\max_{\tilde{g}_{(u_i,s_i,\xi_i)} \in \tilde{\Gamma}} \frac{|\langle R^i f, \tilde{g}_{(u_i,s_i,\xi_i)}\rangle|}{\|\tilde{g}_{(u_i,s_i,\xi_i)}\|^2}. \tag{9}$$

Once $\tilde{\gamma}_i = (u_i, s_i, \xi_i)$ satisfying equation (9) is determined in the space $\tilde{\Gamma}(u, s, \xi)$, the phase shift ϕ_i is now estimated from

$$\phi_i = \arg(\langle R^i f, \tilde{g}_{(u_i,s_i,\xi_i)}\rangle) \tag{10}$$

and the amplitude A_i is simply calculated from its definition:

$$A_i = \frac{|\langle R^i f, \tilde{g}_{(u_i,s_i,\xi_i)}\rangle|}{\|\tilde{g}_{(u_i,s_i,\xi_i)}\|^2}. \tag{11}$$

Phase II. In phase II, the optimal parameter $\gamma_i = (u_i, s_i, \xi_i, \phi_i)$ and the amplitude A_i are determined by the non-linear least squares algorithm utilizing the suboptimal values $(\tilde{\gamma}_i, \phi_i, A_i)$ of phase I as the initial guess. In the application of the matching pursuit algorithm for signal compression, a set of discrete Gabor basis functions is used. Therefore, phase II may be unnecessary. However, the decomposition of the measured wave signal into the optimally selected Gabor functions is important for damage assessment.

To find a set of (γ_i, ϕ_i, A_i) satisfying the following equation:

$$(\gamma_i, \phi_i, A_i) = \arg\min_{\gamma_i \in \Gamma, A_i \in \bar{R}} \|R f^{i+1}\| \tag{12}$$

the standard Gauss–Newton method is employed as a numerical search method. Note that the two phases are used at every iteration.

Consequently, a given wave signal $f(t)$ consisting of M Gabor-shaped multiple echoes can be approximated by the linear combination of the optimally selected M Gabor functions:

$$f(t) \approx \sum_{i=1}^{M} A_i g_{(u_i,s_i,\xi_i,\phi_i)}(t). \tag{13}$$

Then, the parameter sets $\{A_i, u_i, s_i, \xi_i, \phi_i\}_{i=1,\ldots,M}$ can be exploited to extract the damage information. To estimate the crack location and size from experimental results, we will directly use the amplitude A_i and the shift u_i in time $(i = 1, \ldots, M)$. In the next section, the proposed method will be tested numerically.

3. Numerical investigation of the proposed method

In this section, the effectiveness of the proposed method will be first checked for noise robustness. For numerical tests, a signal $f(t)$ consisting of two modulated Gaussian pulses will be used:

$$f(t) = \sum_{i=1}^{2} A_i g_{(u_i,s_i,\xi_i,\phi_i)}(t). \tag{14}$$

If $f(t)$ is corrupted by a Gaussian noise $n(t)$, the noisy signal $\hat{f}(t)$ can be written as

$$\hat{f}(t) = \sum_{i=1}^{2} A_i g_{(u_i,s_i,\xi_i,\phi_i)}(t) + n(t) \tag{15a}$$

where the signal-to-noise ratio (SNR) is given by

$$\mathrm{SNR} = 10\log_{10} \frac{\sum_i |f(t_i)|^2}{\sum_i |n(t_i)|^2} (\mathrm{dB}). \tag{15b}$$

The first case is a simple problem for which the two pulses in $f(t)$ are separated to some distance so they are not overlapped. The specific numerical data used are the following:

$$f(t) = f_1(t) + f_2(t) = \sum_{i=1}^{2} A_i g_{(u_i,s_i,\xi_i,\phi_i)}(t)$$

pulse 1: $A_1 = 1$, $u_1 = 9.906 \times 10^{-5}$ s, $s_1 = 35$, $\xi_1 = 100$ kHz, $\phi_1 = 0$ rad

pulse 2: $A_2 = 0.15$, $u_2 = 29.717 \times 10^{-5}$, $s_2 = 40$, $\xi_2 = 100$ kHz, $\phi_2 = \pi/4$.

The sampling rate is assumed to be $\Delta t = 2 \times 10^{-7}$ s. Figure 3 shows the noisy signal $\hat{f}(t)$ and the signal estimated by the two-phase Gabor pulse-based matching pursuit approach for various SNRs. The estimated values of the parameters are summarized in table 1. From figure 3 and table 1, one can see that the proposed approach gives excellent estimates of $f(t)$ even under small SNRs.

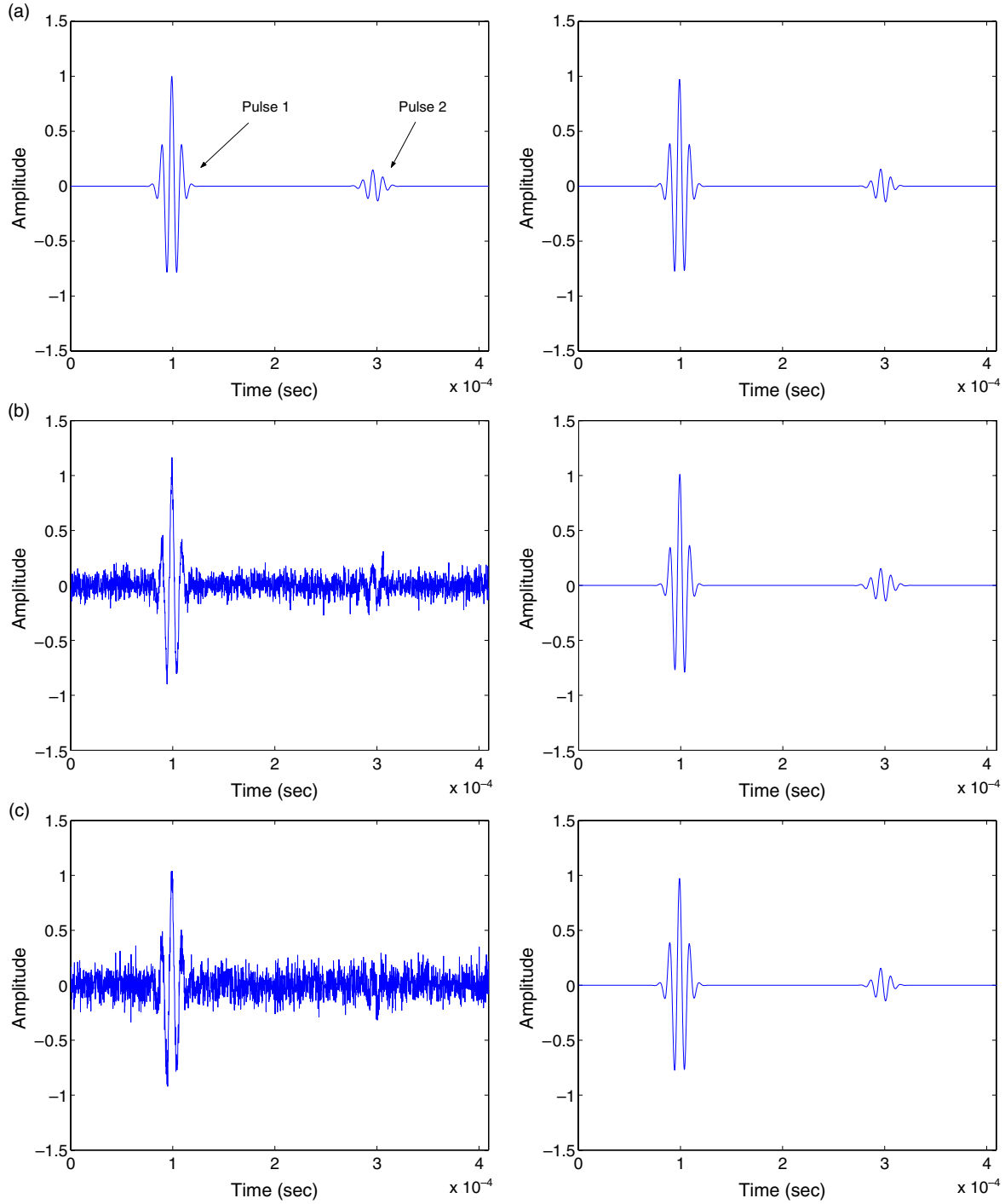

Figure 3. The approximation of the Gabor pulse signals with various SNRs. (a) Noise free, (b) with SNR = 5.1 dB, and (c) with SNR = 1.9 dB (right: noisy $\hat{f}(t)$, left: estimated $f(t)$).

The second case deals with two overlapped pulses. The pulse overlap is observed often in guided-wave inspection, but it is difficult to accurately extract the damage information from measured signals. We use the same pulse forms as were used in the first case but different values of u ($u_1 = 19.821 \times 10^{-5}, u_2 = 21.793 \times 10^{-5}$) in order to overlap two pulses. Figure 4 shows the pulses $f_1(t)$ and $f_2(t)$ estimated by the matching pursuit method, and table 2 gives the numerical values for the estimated parameters. Considering the complexity of the pulse overlap, the parameter estimation is quite satisfactory. In particular, the estimated values of the two parameters $\{A_i, u_i\}_{i=1,2}$, which can be used for the estimation of the crack size and location, are very close to the exact values.

4. Crack identification

In this section, the experimental set-up and the measurement principle of the magnetostrictive transducer are described.

Table 1. The parameter estimation for the numerical case study 1 ($\xi = 100$ kHz).

			A	u ($\times 10^{-5}$ s)	s	ϕ (rad)
Exact values		Pulse 1	1.000	9.906	35.00	0
		Pulse 2	0.150	29.717	40.00	0.785
Estimated values	Noise free	Pulse 1	1.000	9.900	34.99	−0.036
		Pulse 2	0.150	29.720	39.99	0.802
	5.1 dB	Pulse 1	1.013	9.904	34.59	0.081
		Pulse 2	0.155	29.708	41.53	0.708
	1.9 dB	Pulse 1	0.993	9.910	35.78	−0.034
		Pulse 2	0.144	29.841	38.51	0.973

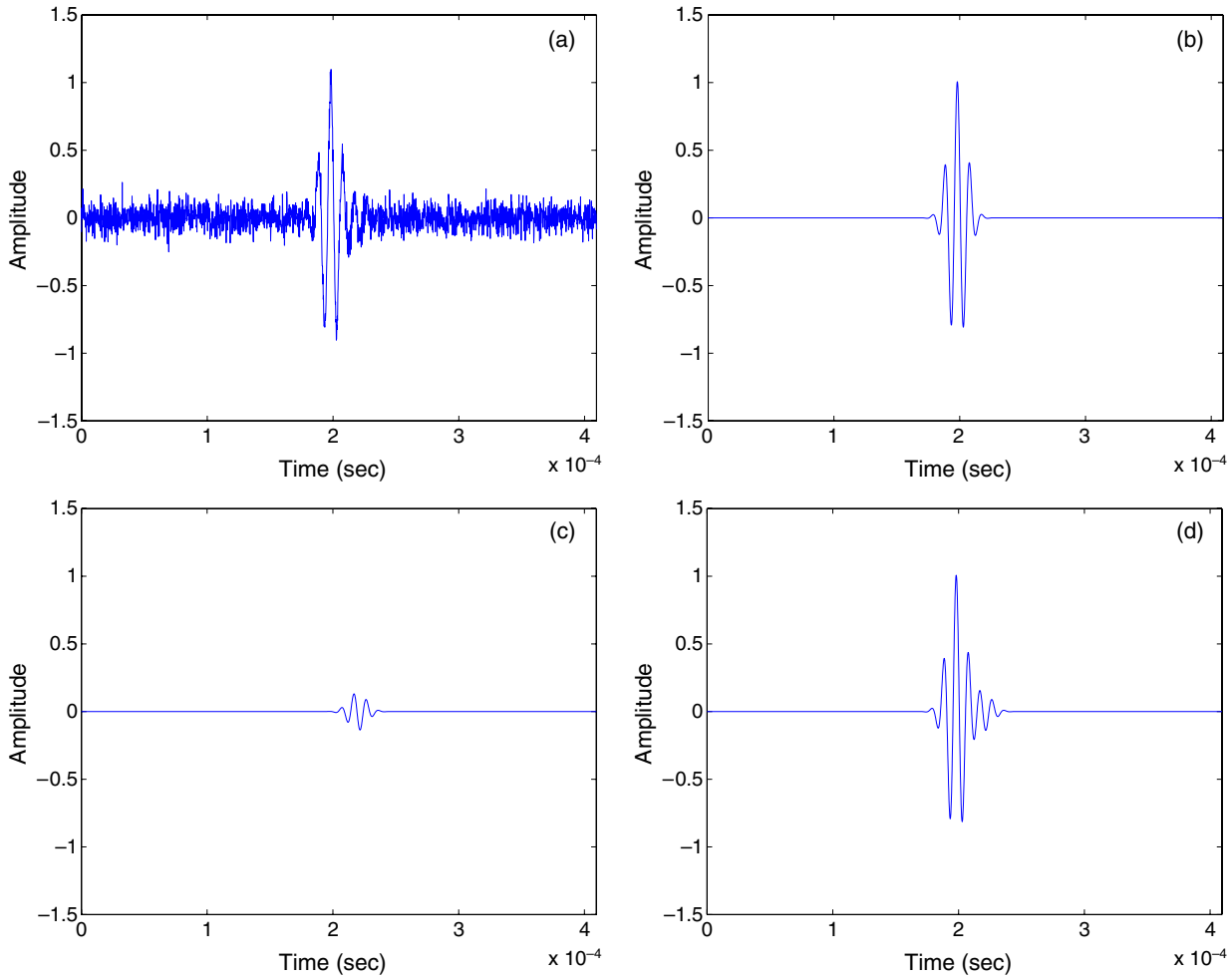

Figure 4. The approximation of the overlapped Gabor pulse signal with SNR = 5.1 dB. (a) Noisy $\hat{f}(t)$, (b) the estimated $f_1(t)$, (c) the estimated $f_2(t)$, and (d) the estimated $f(t) = f_1(t) + f_2(t)$.

Then, the two-phase matching pursuit will be applied to the signals measured in cracked rods. The effectiveness of the proposed method in identifying the location of incident and reflected pulses from noisy signals is shown from analysis results.

4.1. Experimental set-up and measurement principle

Figure 5 shows the experimental set-up employed for the guided-wave-based damage inspection. Figure 6 shows the dimensions of the rod and the crack as well as the transducer location. For the present experiments, magnetostrictive transducers are used, but other transducers are equally applicable. The operation procedure and applications of the magnetostrictive transducer are found in [13, 14]. The transducer at $\bar{A}$ is used as the transmitter and the transducer at $\bar{B}$ as the receiver. With the solenoid-type transducers shown in figure 6, longitudinal waves will be generated. The input pulse from the transmitter is a modulated Gaussian pulse of equation (2) with $\sigma = 40\Delta t = 8 \times 10^{-6}$ s, $\xi = 100$ kHz, and $\phi = 0$ rad. An artificial crack is located at $\bar{C}$, whose depth d varies from 1 to 5 mm and whose width w is 2 mm.

Table 2. The parameter estimation for the numerical case study 2 ($\xi = 100$ kHz).

			A	u ($\times 10^{-4}$ s)	s	ϕ (rad)
Exact values		Pulse 1	1.000	1.981	35	0
		Pulse 2	0.150	2.179	40	0.785
Estimated values	Noise free	Pulse 1	0.998	1.984	36.56	0.204
		Pulse 2	0.147	2.194	34.93	1.801
	7.9 dB	Pulse 1	0.977	1.984	36.72	0.200
		Pulse 2	0.155	2.194	35.52	1.857
	5.1 dB	Pulse 1	1.008	1.982	35.94	0.065
		Pulse 2	0.142	2.196	35.80	1.846

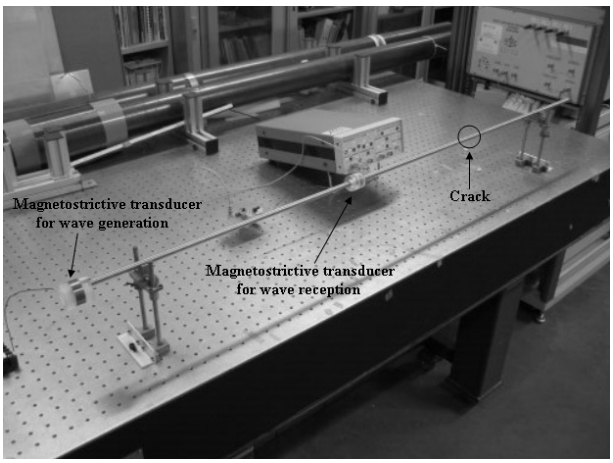

Figure 5. The photo of the experimental set-up.

For later analysis, it is necessary to know the relation between the measured signal from the magnetostrictive transducer and the actual physical quantity. Therefore, the underlying operation principles of the magnetostrictive transducer in generating and measuring waves in ferromagnetic waveguides, known as the Joule effect [15] and the Villari effect [16], will be briefly explained. The Joule effect and the Villari effect can be written as the following two equations when one-dimensional models are employed:

$$\varepsilon = \frac{\sigma}{E^H} + q^* H \tag{16a}$$

$$B = \mu^\sigma H + q\sigma \tag{16b}$$

where ε, σ, B, and H represent strain, stress, magnetic flux density, and magnetic strength, respectively. The material constants E^H, q^*, μ^σ, and q denote the Young's modulus under a constant magnetic strength, the coupling coefficient of the Joule effect, the permeability under a constant stress, and the coupling coefficient of the Villari effect.

When a stress wave is developed in some region of a rod where the solenoid coil of the transducer is encircled, the resulting magnetic state changed by the Villari effect can be picked up by the solenoid coil as the voltage change V:

$$V(x,t) = -\frac{\mathrm{d}\Phi}{\mathrm{d}t} = -N\frac{\mathrm{d}\phi}{\mathrm{d}t} \tag{17}$$

where x is the axial coordinate in figure 6, and N is the turn number of the solenoid coil. The magnetic flux ϕ encircled by one turn of the coil is an integral of the magnetic flux density B over the cross-sectional area A_s enclosed by the solenoid coil. When the applied magnetic field H is time independent, the output voltage can be written as (from equations (16*b*) and (17))

$$V(x,t) = -N\frac{\mathrm{d}}{\mathrm{d}t}\int_{A_s} B\,\mathrm{d}A = -N\frac{\mathrm{d}}{\mathrm{d}t}\int_{A_s} q\sigma\,\mathrm{d}A. \tag{18}$$

In equation (18), if q and σ are assumed to be uniform across the cross-section A_s and if non-linearity and hysteresis are ignored, the magnetostriction coefficient q can be treated simply as a function of x [17–19]:

$$q(x) \approx c(x). \tag{19}$$

Substituting equation (19) into (18) yields

$$V(x,t) \approx -NA_s c(x)\frac{\partial\sigma}{\partial t} \equiv D(x)\frac{\partial\sigma}{\partial t}. \tag{20}$$

Equation (20) states that the measured voltage output V at the transducer is proportional to the time derivative of the axial stress σ.

4.2. Crack identification by the matching pursuit method

To identify the presence of any damage from measured signals and to estimate the crack location, small echoes which may be hidden by measurement noise must be detected. To investigate the effectiveness of the proposed method, guided-wave inspection experiments using the set-up in figure 6 were conducted in cracked rods. Two cracks of $d = 2$ and 3 mm were considered. The signals measured by the transducer for $d = 2$ and 3 mm are plotted in figures 7(a) and (b), respectively.

For the experiments, a Gabor pulse $f_{\mathrm{Gp}}(t)$ with $s = 40$ ($\Delta t = 2\times 10^{-7}$ s), $\xi = 100$ kHz, and $\phi = 0$ rad was generated, but the actual pulse coming from the power amplifier was slightly varied, as shown in figure 8. For accurate analysis of the measured signals at $\bar{B}$, it is important to characterize accurately the waveform of the incident wave going into the rod. Therefore, the matching pursuit algorithm was applied to the signal shown in figure 8, and the three parameters u, s, ϕ were estimated:

$$u = 2.552 \times 10^{-6}\ \mathrm{s}, \qquad s = 40.25, \qquad \phi = 1.608\ \mathrm{rad}.$$

The phase shift was not negligible.

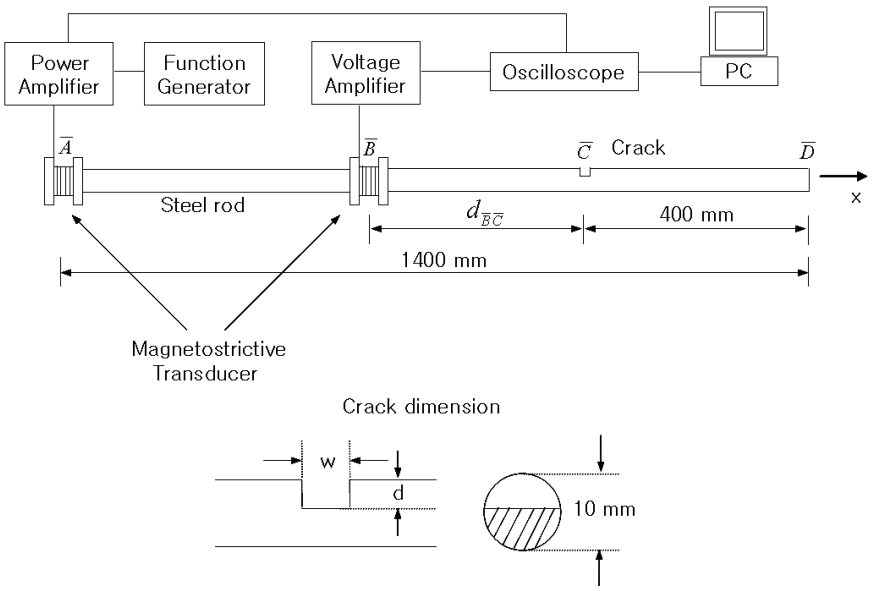

Figure 6. The schematic diagram of the experimental set-up and the dimensions of the test rods.

Table 3. The estimated values of the parameters of the three pulses shown in figure 9 ($\xi = 100$ kHz).

d (mm)		A ($\times 10^{-2}$)	u ($\times 10^{-4}$ s)	s	ϕ (rad)
2	Pulse 1	1.7716	1.246 27	42.94	1.372 01
	Pulse 2	0.1648	2.814 27	38.99	−0.135 40
	Pulse 3	1.5921	4.444 23	44.36	0.901 66
3	Pulse 1	1.7866	1.236 31	43.95	0.568 65
	Pulse 2	0.3387	2.816 26	40.98	−0.820 54
	Pulse 3	1.5035	4.438 25	45.07	0.502 49

Now, the two-phase matching pursuit algorithm is applied to the measured signals in figures 7(a) and (b). The processed results are plotted in figure 9. Both figures 9(a) and (b) clearly show three pulses: the first pulse is the incident wave generated by the transducer at $\bar{A}$; the second small pulse is the wave reflected from the crack $\bar{C}$; the third pulse is the wave reflected from the right end $\bar{D}$. The estimated values of the parameters A and γ are tabulated in table 3. The comparison of figures 7 and 9 shows that the reflected wave from the crack can be clearly identified after the measured signals are processed by the proposed method. Using the estimated parameters u denoting the arrival time of the pulses, the distances $d_{\bar{B}\bar{C}}$ and $d_{\bar{B}\bar{D}}$ between $\bar{B}$ and ($\bar{C}$, $\bar{D}$) are estimated, and the results are compared with the exact values in table 4. In calculating $d_{\bar{B}\bar{C}}$ and $d_{\bar{B}\bar{D}}$, the following formulae are used:

$$\begin{aligned} d_{\bar{B}\bar{C}} &= C_g \times \tfrac{1}{2}(u|_{\text{2nd pulse}} - u|_{\text{1st pulse}}) \\ d_{\bar{B}\bar{D}} &= C_g \times \tfrac{1}{2}(u|_{\text{3rd pulse}} - u|_{\text{1st pulse}}) \end{aligned} \tag{21}$$

where C_g is the group velocity of the longitudinal wave propagating at $\xi = 100$ kHz. (The experimentally determined $C_g = 5018$ m s^{-1} was used for the distance calculation.) As is evident from table 4, the damage location $\bar{C}$ was estimated very accurately.

To see the performance of the proposed matching pursuit approach, a very small crack of $d = 1$ mm is considered. This crack size corresponds to only 5% loss of the cross-sectional area. By repeating the same guided-wave experiment in the cracked rod of $d = 1$ mm, the signal shown in figure 10(a) is obtained. The processed result obtained from the matching pursuit is given in figure 10(b). When the crack size is very small as in this case, however, some meaningless outliers in addition to the reflected pulses from cracks may be extracted because the signal-to-noise ratio is severely low.

Table 4. The estimated distances using the parameter u in table 3 ($(d_{\bar{B}\bar{C}})_{\text{exact}} = 400$ mm, $(d_{\bar{B}\bar{D}})_{\text{exact}} = 800$ mm).

	d (mm)	
	2	3
$(d_{\bar{B}\bar{C}})_{\text{est}}$ (mm)	393.4	396.4
Error (%)	1.7	0.9
$(d_{\bar{B}\bar{D}})_{\text{est}}$ (mm)	802.3	803.4
Error (%)	0.3	0.4

To reduce the effect of noise, the time average of 100 signals was also considered and processed by the matching pursuit method. The results before and after the application of the matching pursuit algorithm are compared in figure 11. Although the magnitude of the pulse reflected from the crack is very small, the proposed method clearly identifies the reflected pulse. The distances $d_{\bar{B}\bar{C}}$ and $d_{\bar{B}\bar{D}}$ estimated by using the parameter u of the pulses shown in figures 10 and 11 are compared in table 5. The use of pulse-dependent basis functions leads to these satisfactory results.

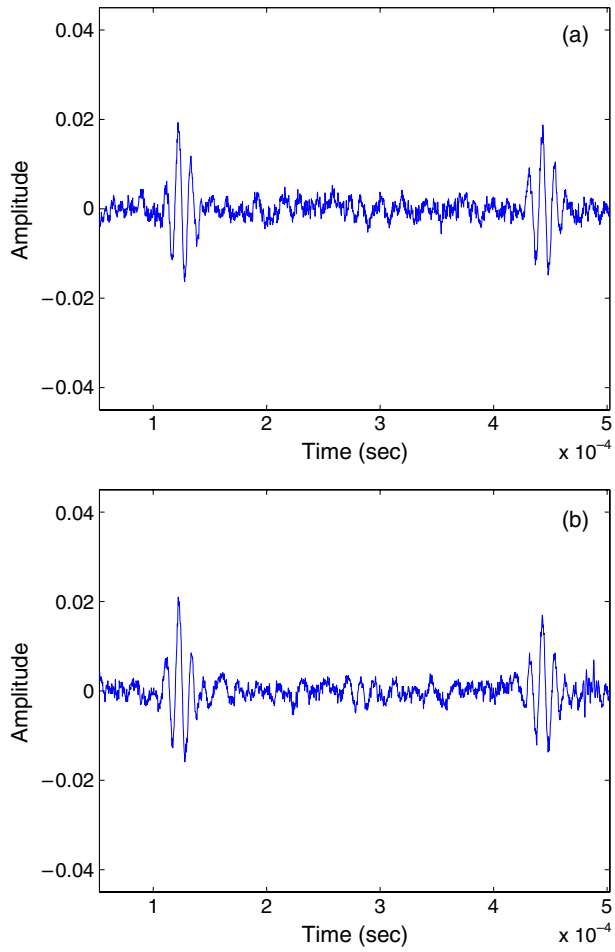

Figure 7. The non-averaged signals measured in the cracked rods (a) of $d = 2$ mm and (b) of $d = 3$ mm.

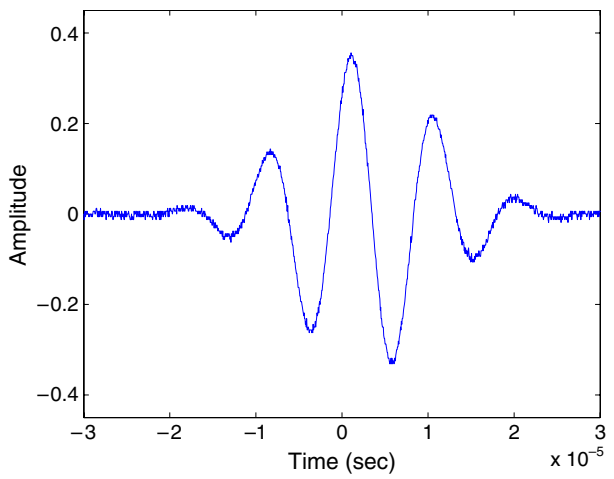

Figure 8. The actual Gabor pulse coming from the power amplifier.

In the next case, the situation where the measured pulses at the receiver overlap each other is considered. This situation could occur when

$$d_{\bar{B}\bar{C}} \leqslant \tfrac{1}{2} C_{\mathrm{g}} T_{\mathrm{support}}^{\mathrm{Incident}} \tag{22}$$

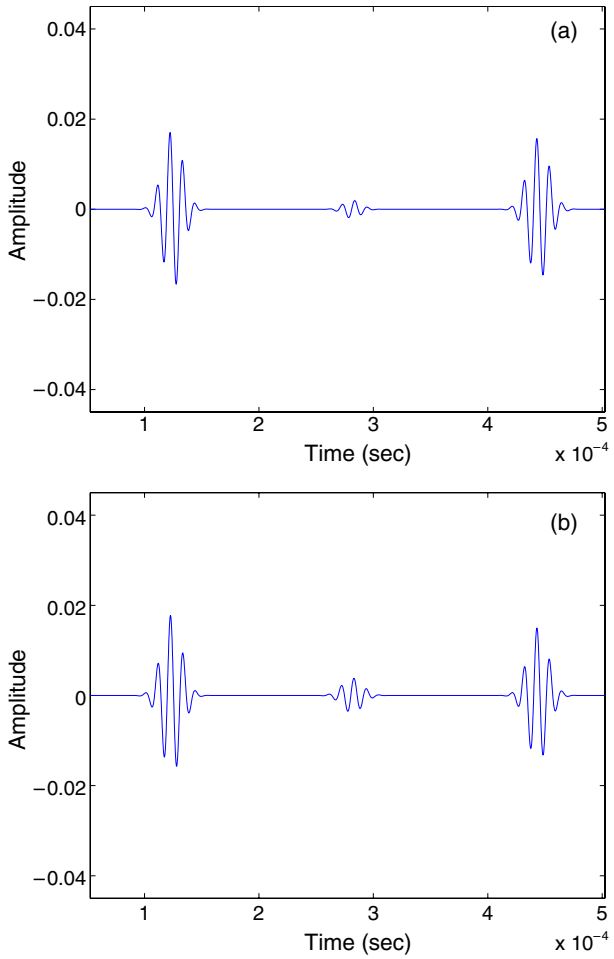

Figure 9. The approximation of the non-averaged signals measured in the cracked rods (a) of $d = 2$ mm and (b) of $d = 3$ mm.

Table 5. The estimated distances for the measured signals for $d = 1$ mm ($(d_{\bar{B}\bar{C}})_{\mathrm{exact}} = 400$ mm, $(d_{\bar{B}\bar{D}})_{\mathrm{exact}} = 800$ mm).

	For non-averaged signal	For 100-averaged signal
$(d_{\bar{B}\bar{C}})_{\mathrm{est}}$ (mm)	414.9	407.4
Error (%)	3.7	1.9
$(d_{\bar{B}\bar{D}})_{\mathrm{est}}$ (mm)	802.8	804.4
Error (%)	0.4	0.5

where $T_{\mathrm{support}}^{\mathrm{incident}}$ denotes the support size of the incident Gabor pulse, which may be approximately by $6s\Delta t$. Using $s = 40$, $C_{\mathrm{g}} = 5018\,\mathrm{m\ s^{-1}}$ (for $\xi = 100\,\mathrm{kHz}$), and $\Delta t = 2\times10^{-7}$ s, (22) becomes

$$d_{\bar{B}\bar{C}} \leqslant 120\ \mathrm{mm}. \tag{23}$$

If condition (23) is met, the incident wave and the wave reflected from the crack at $\bar{C}$ can overlap each other; then, the damage location becomes difficult to assess.

Figures 12(b) and (c) show the pulses obtained by processing the signal measured in figure 12(a). The two pulses are overlapped with each other, but the wave reflected from the crack was distinguished from the incident wave by the proposed method. Table 6 lists the estimated values of $d_{\bar{B}\bar{C}}$.

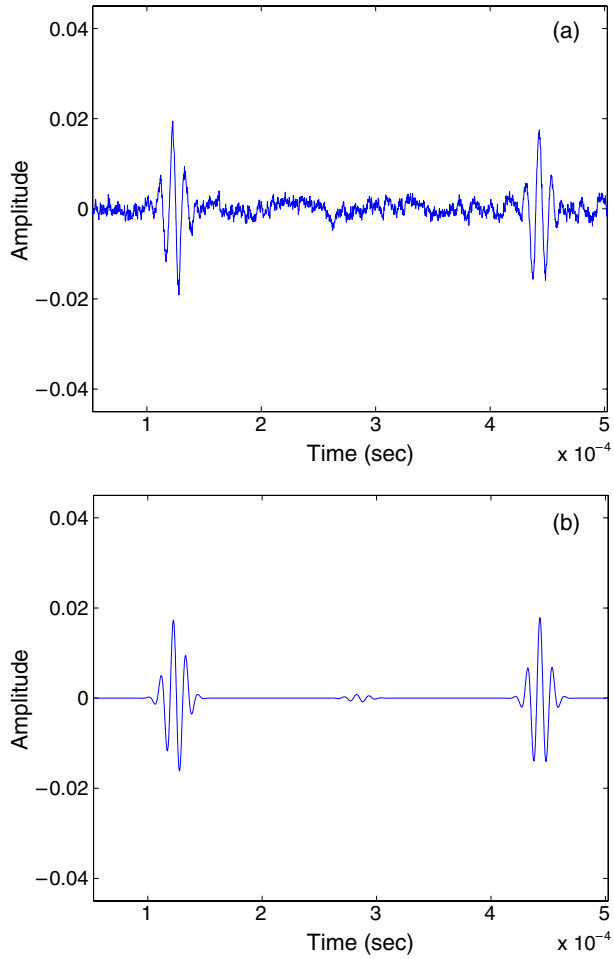

Figure 10. The approximation of the non-averaged signal measured in the rod with the crack of $d = 1$ mm. (a) The measured signal and (b) the approximated signal.

Table 6. The estimated distances for the overlapped pulse signals ($(d_{\bar{B}\bar{C}})_{\text{exact}} = 60$ mm, $(d_{\bar{B}\bar{D}})_{\text{exact}} = 80$ mm).

	d (mm)	
	2	3
$(d_{\bar{B}\bar{C}})_{\text{est}}$ (mm)	62.28	65.80
$(d_{\bar{B}\bar{D}})_{\text{est}}$ (mm)	78.85	80.79

5. Crack size estimation

In the previous section, the Gabor function-based matching pursuit algorithm was successfully applied for damage location estimation. To extend the algorithm further, damage size estimation requiring more information than the damage location estimation will be investigated in this section. To achieve this goal, some analysis regarding the elastic longitudinal wave propagation is also presented.

5.1. Dispersion relation from Love's rod theory

Although the dispersion of longitudinal waves is not so severe, information on the wave dispersion characteristics can improve the accuracy of damage assessment from measured wave signals. The exact dispersion relation, known as the Pochhammer–Chree equation [20–22], is available, but it is better to use a simpler equation for efficient analysis. In this work, the Love theory [20–22] predicting the dispersion relation of the lowest branch of the longitudinal wave is used for damage size estimation.

Unlike the elementary one-dimensional rod theory, Love's theory takes into account lateral motion resulting from Poisson's effect. The equation for the longitudinal displacement $u(x, t)$ from Love's theory is written as

$$EA\frac{\partial^2 u}{\partial x^2} + \nu^2 \rho J \frac{\partial^2 \ddot{u}}{\partial x^2} - \rho A \frac{\partial^2 u}{\partial t^2} = 0 \tag{24}$$

where E, A, ν, ρ, J denote the Young's modulus, the cross-sectional area of the rod, Poisson's ratio, the density, and the polar moment of the cross-section, respectively. The relation between the wavenumber k and the angular frequency ω, and the frequency-dependent group velocity $C_{\text{g}}(\omega)$ can be derived from equation (24) as

$$k = \omega \sqrt{\frac{\rho A}{EA - \nu^2 \rho J \omega^2}} \tag{25a}$$

$$C_{\text{g}}(\omega) = \sqrt{\frac{E}{\rho}} \left[1 - \nu^2 \frac{\rho J \omega^2}{EA} \right]^{\frac{3}{2}}. \tag{25b}$$

In deriving equation (25*a*), the longitudinal displacement u is assumed as

$$u(x, t) = A e^{\text{j}(\pm kx + \omega t)}.$$

Figure 13 compares the group velocity C_{g} given by Love's theory with that given by the exact Pochhammer–Chree theory and shows that Love's theory gives satisfactory results in the frequency range of interest to us (around $\xi = 100$ kHz).

5.2. Theoretical model for wave reflection from a crack

To estimate the crack size from the measured wave signal, the wave mechanics regarding reflection and transmission should be understood. Here, a one-dimensional analysis will be carried out based on the model shown in figure 14. Assuming two waves propagating to the left and the right in each section of figure 14, the longitudinal displacement u_i in each section can be written as

$$u_i(x, t) = A_i e^{-j(k_1 x - \omega_1 t)} + B_i e^{\text{j}(k_1 x + \omega_1 t)} \qquad (i = 1, 2, 3). \tag{26}$$

The wavenumber–frequency relation for equation (26) is given by equation (25*a*). In section 1, the A_1-term in equation (26) corresponds to the incident wave whereas the B_1-term corresponds to the reflected wave. At crack boundaries, the continuity conditions of the displacement and the following stress yield the ratio $R(w; d) = B_1/A_1$:

$$\sigma = E\frac{\partial u}{\partial x} + \frac{1}{2}\nu^2 \rho r^2 \frac{\partial \ddot{u}}{\partial x} \tag{27}$$

where r is the radius of the rod. If the incident wave and the reflected wave from the crack are extracted by the matching pursuit algorithm, the ratio $R(w; d) = B_1/A_1$ can be used to estimate the crack size. The magnitude of $|R(w; d)|_{\text{theory}}$ is

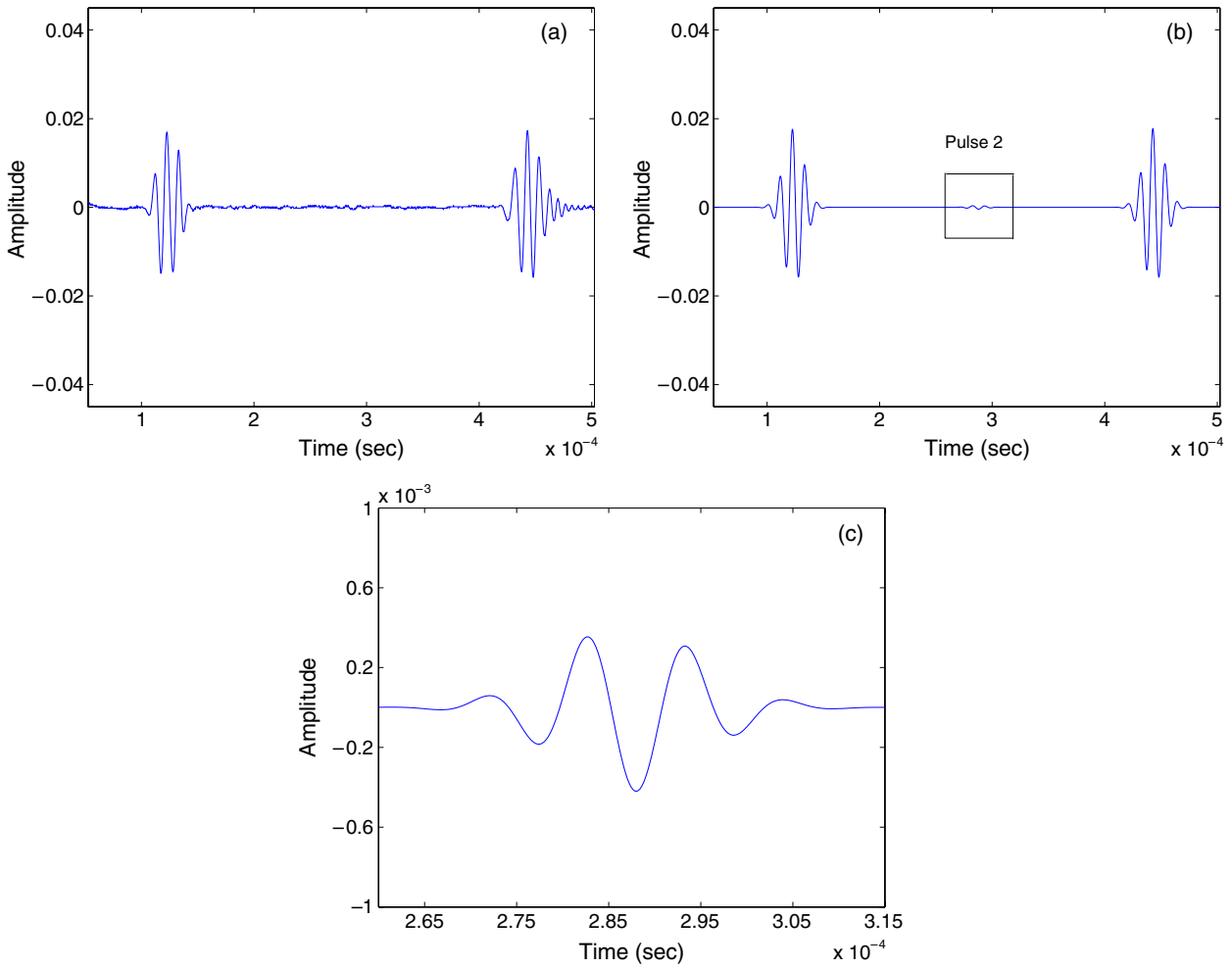

Figure 11. The approximation of the 100-averaged signal measured in the rod with the crack of $d = 1$ mm. (a) The measured signal, (b) the approximated signal, and (c) the zoomed pulse 2.

plotted in figure 15 as a function of d for some values of w. This ratio varies substantially according to the crack depth d and width w.

To find how the voltage signal $V(x_0, t)$ measured by the magnetostrictive transducer is correlated with the coefficients A_1 and B_1, consider a measured signal $V(x_0, t)$ which is split into two parts, $V_{\text{inc}}(x_0, t)$ and $V_{\text{ref}}^{\text{crack}}(x_0, t)$, by the matching pursuit approach. The voltage output $V_{\text{inc}}(x_0, t)$ of the incident wave $u_{\text{inc}}(x, t) = A_1 \text{e}^{-\text{j}(k_1 x - \omega_1 t)}$ can be obtained as

$$\begin{aligned} V_{\text{inc}}(x_0, t) &= D(x_0) \frac{\partial \sigma_{\text{inc}}}{\partial t} \\ &= D(x_0) \frac{\partial}{\partial t} \left(E \frac{\partial u_{\text{inc}}}{\partial x} + \frac{1}{2} \nu^2 \rho R^2 \frac{\partial \ddot{u}_{\text{inc}}}{\partial x} \right) \\ &= D(x_0) \left[E k_1 \omega_1 - \tfrac{1}{2} \nu^2 \rho r^2 k_1 \omega_1^3 \right] A_1 \text{e}^{-\text{j}(k_1 x_0 - \omega_1 t)} \end{aligned} \tag{28}$$

where equations (20) and (27) are used. Likewise, the voltage output $V_{\text{ref}}^{\text{crack}}(x_0, t)$ from the reflected wave $u_{\text{ref}}^{\text{crack}}(x, t) = B_1 \text{e}^{\text{j}(k_1 x + \omega_1 t)}$ from the crack is

$$\begin{aligned} V_{\text{ref}}^{\text{crack}}(x_0, t) &= D(x_0) \frac{\partial \sigma_{\text{ref}}^{\text{crack}}}{\partial t} \\ &= -D(x_0) \left[E k_1 \omega_1 - \tfrac{1}{2} \nu^2 \rho r^2 k_1 \omega_1^3 \right] B_1 \text{e}^{\text{j}(k_1 x_0 + \omega_1 t)}. \end{aligned} \tag{29}$$

From equations (28) and (29), the following relation is obtained:

$$\frac{|V_{\text{ref}}^{\text{crack}}(x_0, t)|_{\max}}{|V_{\text{inc}}(x_0, t)|_{\max}} = \frac{|B_1|}{|A_1|} = |R(w; d)|. \tag{30}$$

When the Gabor pulse is used in the experiment, the amplitudes of the incident and reflected waves that can be estimated using equation (12) from the matching pursuit can be directly used to obtain $|R(w; d)|_{\text{exp}}$.

5.3. Application of the matching pursuit approach

To correlate $\left[\frac{|V_{\text{ref}}^{\text{crack}}(x_0,t)|_{\max}}{|V_{\text{inc}}(x_0,t)|_{\max}}\right]_{\text{exp}}$ with $|R(w; d)|_{\text{theory}}$, measured signals for $d = 1$ mm to 5 mm including the already available signals were used. The matching pursuit algorithm described earlier was applied to these signals for the estimation of the parameter γ and the amplitude A. The result $|R(w; d)|_{\text{exp}}$ determined from the experimental data is plotted as a solid line in figure 15. Table 7 summarizes the crack size estimated by the comparison of $|R(w; d)|_{\text{exp}}$ and $|R(w; d)|_{\text{theory}}$. The deviation of the present estimation from the exact value is small; the proposed matching pursuit approach based on the Gabor dictionary appears to be quite satisfactory.

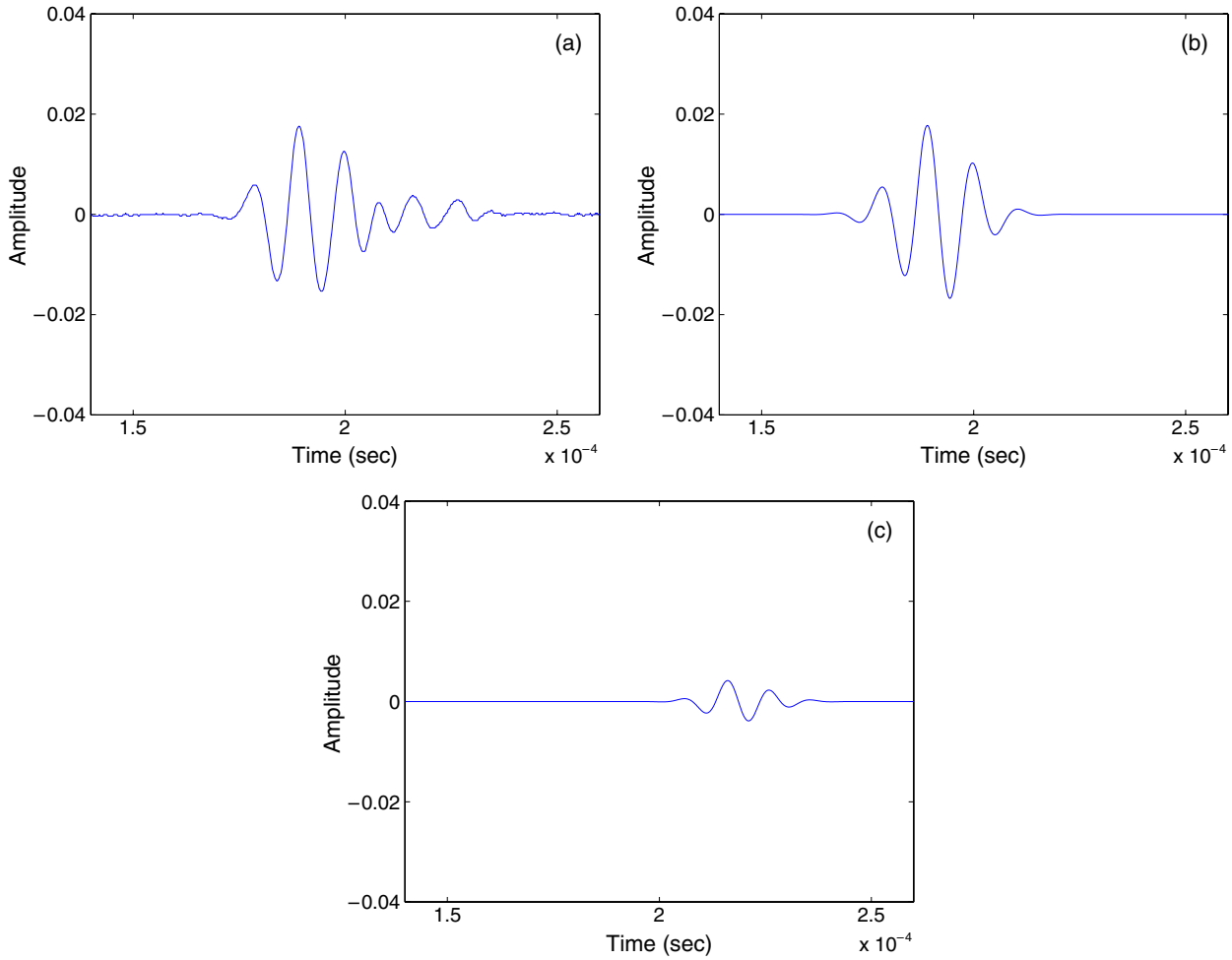

Figure 12. The approximation of the overlapped pulse signal measured in the cracked rod ($d = 3$ mm, $d_{\bar{B}\bar{C}} = 60$ mm). (a) The overlapped pulse, (b) incident pulse ($u = 1.922 \times 10^{-4}$ s), and (c) the reflected pulse ($u = 2.184 \times 10^{-4}$ s).

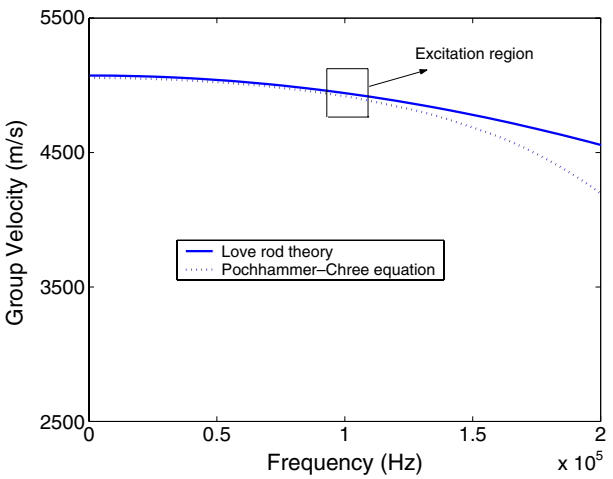

Figure 13. The comparison of the dispersion curve given by Love's theory and that given by the 3D exact equation.

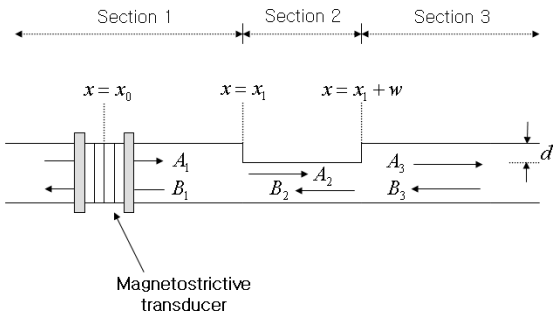

Figure 14. One-dimensional model for incident, reflected, and transmitted waves in a rod having a crack with width w and depth d.

Table 7. The crack sizes estimated by the proposed approach.

	d (mm)				
	1	2	3	4	5
$(d)_{\text{est}}$ (mm)	1.25	2.25	3.40	4.50	5.45

6. Conclusions

A two-stage matching pursuit approach was proposed to estimate the location and size of a crack from longitudinal wave signals measured in cracked rods. The proposed method successfully extracted meaningful pulses from measured noisy

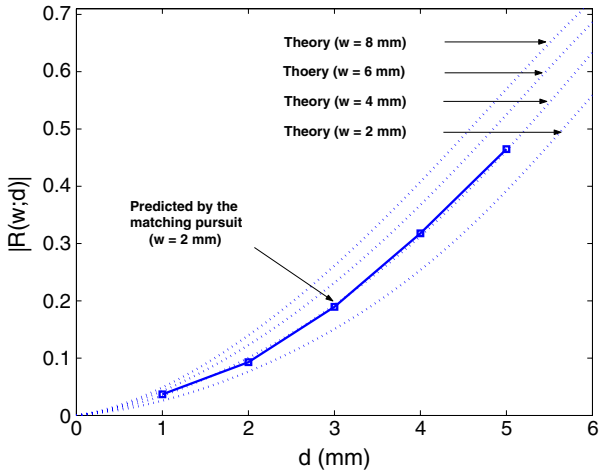

Figure 15. The comparison of the reflection coefficients found by the experiments ($w = 2$ mm) and those from the theory.

signals. Very small echoes reflected from a crack, which would be difficult to detect by other methods, were captured by the approach. The successful application of the present method in the guided-wave inspection problem was partly due to the good choice of the matching pursuit dictionary; the dictionary consisted of Gabor functions having excellent energy concentration both in time and in space. To more adaptively utilize the matching pursuit algorithm in actual experiments, the Gabor pulses, instead of commonly used truncated sine pulses, were used.

References

[1] Rose J L, Ditri J J, Pilarski A, Rajana K and Carr F T 1994 A guided wave inspection techniques for nuclear stream generator tubing *NDT E Int.* **27** 307–30

[2] Cawley P and Alleyne D 1996 The use of Lamb waves for the long range inspection of large structures *Ultrasonics* **34** 287–90

[3] Ghosh T, Kundu T and Karpur P 1998 Efficient use of Lamb modes for detecting defects in large plates *Ultrasonics* **36** 791–801

[4] Lemistre M and Balageas D 2001 Structural health monitoring system based on diffracted Lamb wave analysis by multiresolution processing *Smart Mater. Struct.* **10** 504–11

[5] Kessler S S, Spearing S M and Soutis C 2002 Damage detection in composite materials using Lamb wave methods *Smart Mater. Struct.* **11** 269–78

[6] Hertz D 1986 Time delay estimation by combining efficient algorithms and generalized cross-correlation methods *IEEE. Trans. Acoust. Speech Signal Process.* **34** 1–7

[7] Grennberg A and Sandell M 1994 Estimation of subsample time delay differences in narrowband ultrasonic echoes using the Hilbert transform correlation *IEEE Trans. Ultrason. Ferroelectr. Freq. Control* **41** 588–95

[8] Li Y T and Kurkjian A L 1983 Arrival time determination using iterative signal reconstruction from the phase of the cross spectrum *IEEE Trans. Acoust. Speech Signal Process.* **31** 502–4

[9] Mallat S and Zhang Z 1993 Matching pursuits with time–frequency dictionaries *IEEE Trans. Signal Process.* **41** 3397–415

[10] Zhang G, Zhang S and Wang Y 2000 Application of adaptive time–frequency decomposition in Ultrasonic NDE of highly scattering materials *Ultrasonics* **38** 961–4

[11] Ruiz N, Vera P, Curpian J, Martinez D and Mata R 2003 Matching pursuit-based signal processing method to improve ultrasonic flaw detection in NDT applications *Electron. Lett.* **39** 413–4

[12] Gabor D 1946 Theory of communication *J. Inst. Electr. Eng.* **93** 429–57

[13] Kwun H and Teller C M 1994 Magnetostrictive generation and detection of longitudinal, torsional, and flexural waves in a steel rod *J. Acoust. Soc. Am.* **96** 1202–4

[14] Kwun H and Bartel K A 1998 Magnetostrictive sensor technology and its applications *Ultrasonics* **36** 171–8

[15] Joule J P 1847 On the effect of magnetism upon the dimensions of iron and steel bars *Phil. Mag.* III **30** 76

[16] Villari E 1865 Change of magnetization by tension and by electric current *Ann. Phys. Chem.* **126** 87–122

[17] Lee H C and Kim Y Y 2002 Wave selection using a magnetomechanical sensor in a solid cylinder *J. Acoust. Soc. Am.* **112** 953–60

[18] Cho S H, Kim Y and Kim Y Y 2003 The optimal design and experimental verification of the bias magnet configuration of a magnetostrictive sensor for bending wave measurement *Sensors Actuators* A **107** 225–32

[19] Kim Y Y, Park C I, Cho S H and Han S W 2005 A new magnetostrictive transducer for torsional waves in cylindrical waveguides and its applications *J. Acoust. Soc. Am.* at press

[20] Miklowitz J 1978 *Elastic Waves and Waveguides* (New York: North-Holland)

[21] Graff K F 1975 *Wave Motion in Elastic Solids* (Columbus, OH: Ohio State University Press)

[22] Doyle J F 1997 *Wave Propagation in Structures* (New York: Springer)